Physics of the Earth and Planetary Interiors, 36 (1984) 224–235
Elsevier Science Publishers B.V., Amsterdam – Printed in The Netherlands

The strength of intraplate lithosphere

N.J. Kusznir and R.G. Park

Department of Geology, University of Keele, Keele, Staffs. ST5 5BG (Gt. Britain)

(Received November 23, 1983; revision accepted May 23, 1984)

Kusznir, N.J. and Park, R.G., 1984. The strength of intraplate lithosphere. Phys. Earth Planet. Inter., 36: 224–235.

The deformation of intraplate lithosphere in response to laterally applied stress has been investigated using a mathematical model of the elastic, brittle and viscous response of the lithosphere. Fundamental to the model is the conservation of the horizontal force associated with the applied stress and the redistribution of stress within the lithosphere after stress release by ductile or brittle failure. Ductile deformation is assumed to be controlled by dislocation creep in quartz in the crust and by dislocation and Dorn law creep in olivine in the mantle. Brittle failure is predicted using Griffith theory. The redistribution of stress after brittle and ductile deformation results in large levels of stress in the middle and lower crust immediately above the elastic–ductile or brittle–ductile transition.

Lithosphere deformation is controlled critically by the lithosphere thermal structure of which surface heat flow, q, is taken as a convenient indicator. For hotter lithosphere, stress release by ductile deformation in the middle and lower lithosphere is more extensive and rapidly leads to larger levels of stress in the upper lithosphere. For sufficiently large levels of applied stress, or sufficiently hot lithosphere, complete failure (*Whole Lithosphere Failure*) of the lithosphere occurs by ductile and brittle deformation resulting in geologically significant strains.

Critical levels of applied stress required to produce *Whole Lithosphere Failure* have been computed as a function of the lithosphere surface heat flow. The predicted strength of the lithosphere has been compared with expected levels of intraplate stress arising from plate boundary forces and isostatically compensated loads. The model predicts significant extensional intraplate deformation in regions of moderate heat flow with $q > 60$ m W m^{-2}. For compressional deformation, however, a hotter lithosphere is required with $q >$ c. 75 m W m^{-2}. The model predictions are in general agreement with the comparatively widespread occurrence of extensional intraplate deformation and the restricted occurrence of compressional deformation.

The model has also been used to investigate the relationship between the depth of the brittle–ductile transition and lithosphere temperature structure. The brittle–ductile transition depth is shown to become shallower with increasing heat flow, in good agreement with seismic evidence.

1. Introduction

The lithosphere plate was regarded originally as part of a strong layer showing no significant internal lateral distortion over time periods of the order of tens of Ma. However, more recent studies, stimulated in part by the conceptual model of McKenzie (1978), have emphasized the importance of intraplate extensional tectonics in the formation of graben, rifts and sedimentary basins found within all the major continental plates. Compressional intraplate tectonics in contrast appears to be much less common: well known examples are the compressional fold and thrust belts situated within the Asian plate north of the Himalayan collision zone between India and Asia (Molnar and Tapponnier, 1975). Oceanic intraplate deformation appears to be neither pervasive nor extensive, being generally confined to brittle deformation in the upper crust associated with insignificant strains, or to lithosphere flexure associated with sediment or seamount loading (e.g., Bodine et al., 1981).

The magnitude of the stresses involved in intraplate deformation must clearly be large enough to promote frequent though localized extensional failure in continental lithosphere but too small for compressional failure except under occasional circumstances.

The sources and distribution of tectonic stress

0031-9201/84/$03.00

TABLE I

Contributions to tectonic stress

Source of tectonic stress	Expected stress magnitude distributed over lithosphere	
	in oceanic [+] lithosphere	in continental [x] lithosphere
Plate boundary forces		
(a) Ridge push	0.2–0.3 kbar (compression)	0.1–0.15 kbar (compression)
(b) Slab pull *	0–0.5 kbar (mainly tension)	0–0.25 kbar (mainly tension)
(c) Subduction suction	0–0.3 kbar (tension)	0–0.15 kbar (tension)
Compensated load forces		
(a) Continental margin	normally 0 (but up to 0.2 kbar compression)	0.1 kbar (tension)
(b) Plateau uplift	–	0–0.3 kbar (tension)

* Slab pull stress is the net resultant of slab pull, subduction resistance and collision resistance forces.

[+] For oceanic lithosphere—80 km thick.

[x] For continental lithosphere—150 km thick.

in the lithosphere have been investigated by Forsyth and Uyeda (1975), Turcotte and Oxburgh (1976) and Richardson et al. (1976). The most important sources responsible for significant tectonic stress arise from plate boundary forces and from isostatically compensated loads (Bott and Kusznir, 1984). Table I summarizes the sources and estimated stress levels. The average stress levels within the present continental plates arising from these sources seem likely to lie within the range $-0.25-+0.25$ kbar, if distributed over the whole lithosphere plate. However, measured and calculated stresses in the upper and middle parts of the crust are larger—Heard (1976) suggested a localised maximum value for the stress difference of 2–3 kbars.

This apparent discrepancy is explained by the redistribution of stress after ductile creep in the lower lithosphere. This redistribution of stress leads to large levels of stress in the brittle upper lithosphere—stress levels sufficient to cause fracture. This process has been named stress amplification and has been investigated by Kusznir and Bott (1977), Bott and Kusznir (1979), Kusznir (1982), Mithen (1982) and Kusznir and Park (1982, 1984). Figure 1A schematically shows the stress amplification process.

Fracture in the upper lithosphere also leads to stress release and its redistribution. This generates even greater stresses in the remaining competent lithosphere. For sufficiently large levels of applied stress, the whole of the brittle lithosphere may fracture. This situation in which all of the lithosphere has suffered either ductile or brittle deformation is called *Whole Lithosphere Failure* (WLF) and is illustrated in Fig. 1B. A cyclic process of upper lithosphere fracture and lower lithosphere creep then occurs as the stress is transferred between upper and lower lithosphere. Only after WLF can extensive lithosphere deformation with large horizontal strains take place.

The deformation will in turn alter both the geometry and the rheology of the lithosphere. Thus extensional thinning may be accompanied by the emplacement of warmer lithosphere material and by the development of vulcanicity which will lead to further structural weakening. Thermal weakening may either be a consequence or an important contributory cause of extensional failure. By investigating critical strength for different thermal regimes, the model can be used to suggest which of these alternatives is likely in particular examples.

2. The mathematical formulation of the lithosphere deformation model

The mathematical model of intraplate deformation analyses the elastic, ductile and brittle response of intraplate lithosphere when subjected to a lateral applied stress. It is assumed that the sources of the laterally applied stress are plate boundary forces and isostatically compensated loads. Such forces will persist even when intraplate lithosphere deformation occurs and the stresses so generated have been named renewable stresses by Bott and Kusznir (1984). A fundamental feature of the model is the conservation of the horizontal force carried by the lithosphere arising from the applied stress. As a consequence the model incorporates the stress release and transfer after ductile and brittle deformation.

Figure 2 shows the coordinate system of the

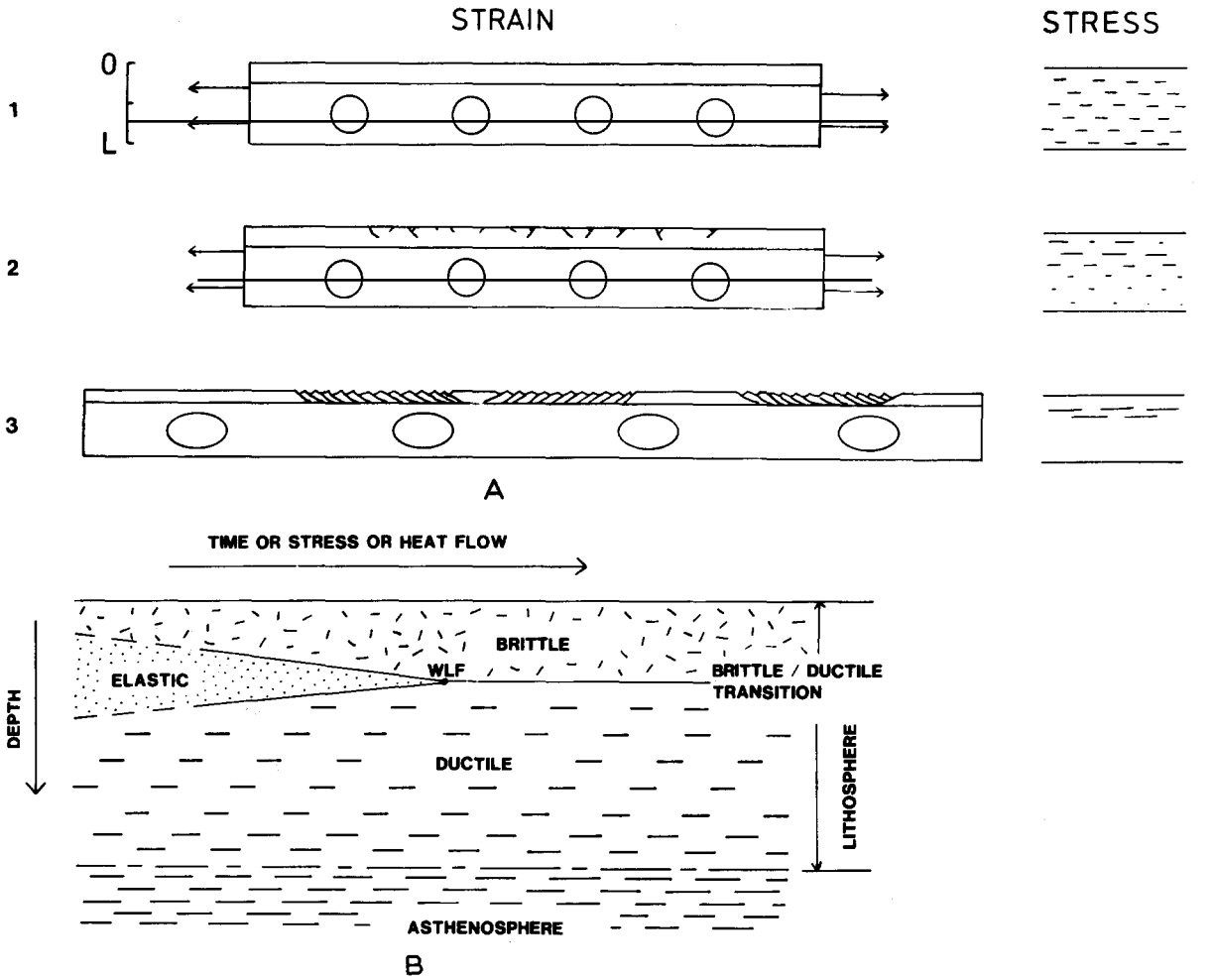

Fig. 1. (A) A schematic representation of lithosphere response to an applied horizontal stress. (1) Initial elastic response of the lithosphere. Strains and stresses are uniformly distributed with depth through the lithosphere. (2) Ductile creep in the lower lithosphere causes stress decay there. Stress transfer results in amplification in the upper lithosphere. Stress levels in the uppermost lithosphere may be sufficient to cause fracture. (3) Stress amplification may result in large stress levels in the upper lithosphere sufficient to cause complete failure of the brittle lithosphere. *Whole Lithosphere Failure* (WLF) then occurs leading to geologically significant horizontal strains in the lithosphere. (B) The regions of brittle, ductile and elastic behaviour in the lithosphere shown diagramatically. Given a large enough applied stress the elastic core will reduce to zero with time as the brittle and ductile deformation extends downwards and upwards, respectively. WLF occurs when the elastic layer disappears. Increasing heat flow has the same effect as increasing stress.

model. The externally derived applied stress σ_0 is applied initially over the whole lithosphere thickness, in the x direction. Plane strain is assumed to exist in the y direction (i.e., $\varepsilon_y = 0$) and the stress σ_z arising from the applied stress σ_0 is assumed to be zero (i.e., $\sigma_z = 0$).

Conservation of the horizontal force arising from the applied stress σ_0 gives the equation

$$\int_0^L \sigma_x \mathrm{d}z = \text{constant} \qquad (1)$$

where σ_x is the horizontal stress in the x direction and L is the lithosphere thickness. The assumption that the various layers of the lithosphere are welded

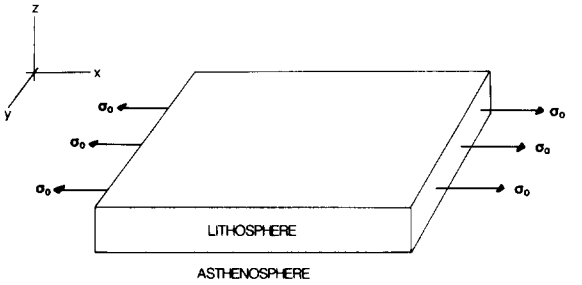

Fig. 2. The lithosphere model showing the coordinate scheme.

together gives the equation

$$\frac{d\varepsilon_x}{dz} = 0 \tag{2}$$

where ε_x is the total strain in the x direction.

Differentiation of eqs. 1 and 2 with time gives

$$\int_0^L \dot{\sigma}_x dz = 0 \tag{3}$$

and

$$\frac{d\dot{\varepsilon}_x}{dz} = 0$$

The behaviour of each component element of the lithosphere material is assumed to be that of a Maxwell visco-elastic material. Strains ε_x, ε_y and ε_z and stresses σ_x, σ_y and σ_z are consequently linked by the equations

$$\varepsilon_x = \frac{1}{E}(\sigma_x - \sigma_x^0) - \frac{\nu}{E}(\sigma_y - \sigma_y^0) - \frac{\nu}{E}(\sigma_z - \sigma_z^0) + \varepsilon_x^v$$

$$\varepsilon_y = \frac{1}{E}(\sigma_y - \sigma_y^0) - \frac{\nu}{E}(\sigma_x - \sigma_x^0) - \frac{\nu}{E}(\sigma_z - \sigma_z^0) + \varepsilon_y^v$$

$$\varepsilon_z = \frac{1}{E}(\sigma_z - \sigma_z^0) - \frac{\nu}{E}(\sigma_x - \sigma_x^0) - \frac{\nu}{E}(\sigma_y - \sigma_y^0) + \varepsilon_z^v \tag{4}$$

σ_x^0, σ_y^0 and σ_z^0 are initial stresses and ε_x^v, ε_y^v and ε_z^v are creep strains. E is Young's modulus and ν Poisson's ratio.

The creep strain rate $\dot{\varepsilon}_x^v$ is given by the equation

$$\dot{\varepsilon}_x^v = \frac{(2\sigma_x - \sigma_y - \sigma_z)}{6\eta} \tag{5}$$

and similarly for $\dot{\varepsilon}_y^v$ and $\dot{\varepsilon}_z^v$. η is the apparent viscosity.

Manipulation of eqs. 4 and 5 with the additional equations $\varepsilon_y = 0$ and $\sigma_z = 0$ gives

$$\dot{\varepsilon}_x = \frac{(1-\nu^2)}{E}(\dot{\sigma}_x - \dot{\sigma}_x^0) + \frac{(2\sigma_x - \sigma_y)}{6\eta} + \nu\frac{(2\sigma_y - \sigma_x)}{6\eta} \tag{6}$$

Further manipulation of this equation with eq. 3 gives

$$\dot{\sigma}_x = \frac{1}{L}\int_0^L k\dot{\varepsilon}_v dz - k\dot{\varepsilon}_v - \frac{1}{L}\int_0^L \dot{\sigma}_x^0 dz + \dot{\sigma}_x^0 \tag{7}$$

and

$$\dot{\sigma}_y = \nu(\dot{\sigma}_x - \dot{\sigma}_x^0) - E\frac{(2\sigma_y - \sigma_x)}{6\eta} + \dot{\sigma}_y^0 \tag{8}$$

where

$$k = E/(1-\nu^2)$$

and

$$\dot{\varepsilon}_v = \frac{\sigma_x(2-\nu) - \sigma_y(1-2\nu)}{6\eta}$$

Integration of eqs. 7 and 8 gives

$$\sigma_x = \int_0^t \left(\frac{1}{L}\int_0^L k\dot{\varepsilon}_v dz - k\dot{\varepsilon}_v\right)dt' - \frac{1}{L}\int_0^L \sigma_x^0 \cdot dz + \sigma_x^0 \tag{9}$$

$$\sigma_y = \int_0^t \left(\nu\dot{\sigma}_x - E\frac{(2\sigma_y - \sigma_x)}{6\eta}\right)dt' + \sigma_y^0 - \nu\sigma_x^0 \tag{10}$$

The starting condition is $\sigma_x(t=0) = \sigma_0$.

The values of E and ν used for the lithosphere are 1.7×10^{11}Pa and 0.25, respectively.

Ductile deformation within the continental lithosphere is assumed to be controlled by the ductile deformation of olivine in the mantle and quartz in the crust. After Goetze (1978) the ductile deformation of olivine is assumed to correspond to dislocation creep at low stresses and Dorn law at higher stresses. Both mechanisms are strongly temperature and stress dependent.

The equations for the creep rates for olivine are taken from Bodine et al. (1981) and represent a compromise between the dry olivine creep rates of Goetze (1978) and the wet dunite creep rates of Post (1977).

Dislocation creep

$$\dot{\varepsilon} = 7 \times 10^{10} \exp\left(\frac{-53030.3}{T}\right)(\sigma_1 - \sigma_3)^3 \text{ s}^{-1}$$

for $(\sigma_1 - \sigma_3) < 2$ kbar

Dorn Law

$$\dot{\varepsilon} = 5.7 \times 10^{11} \exp\left(\frac{-55555.6}{T} \left(1 - \frac{(\sigma_1 - \sigma_3)}{85} \right)^2 \right)$$

s^{-1} for $(\sigma_1 - \sigma_3) > 2$ kbar

where $\sigma_1 - \sigma_3$ is in kbar (1 kbar = 100 MPa).

The ductile deformation of quartz within the crust is assumed to correspond to that of dislocation creep. Creep rates in quartz are controlled strongly by the amount of water. The continental upper crust is assumed to deform according to a wet quartz rheology with 50% quartz. The lower crust is assumed to deform according to a dry quartz rheology with 10% quartz. Creep rates for wet and dry quartz are based on the experimental work of Koch et al. (1980).

Wet quartz

$$\dot{\varepsilon} = 4.36 \exp\left(\frac{-19332.08}{T} \right) (\sigma_1 - \sigma_3)^{2.44} \ s^{-1}$$

Dry quartz

$$\dot{\varepsilon} = 0.126 \exp\left(\frac{-18244.65}{T} \right) (\sigma_1 - \sigma_3)^{2.86} \ s^{-1}$$

where $(\sigma_1 - \sigma_3)$ is in kbar.

Brittle deformation which occurs within the upper lithosphere is incorporated in the model by means of the initial stress parameter σ^0. Brittle fracture is predicted using Griffith theory as modified by McClintock and Walsh (1962). Three failure domains are used; tensional, open crack compressional and closed crack compressional failure. Failure is dependent on stresses σ_x and σ_z. On failure the stress σ_x is returned to the failure envelope; the stress σ_z is simply lithostatic. The values of tensile strength T_0, the frictional coefficient μ and the critical stress required to close cracks σ_{gc}, used to predict failure are $T_0 = 20$ MPa, $\mu = 0.5$ and $\sigma_{gc} = 100$ MPa. The choice of the numerical values for T_0, μ and σ_{gc} is discussed by Kusznir and Park (1984) together with the effect of varying T_0 and μ.

The ductile deformation within the lithosphere is strongly dependent on lithosphere temperature. As a consequence the temperature structure of the lithosphere plays an important part in controlling lithosphere deformation. The temperature structure of the continental lithosphere model has been calculated using a model based on Pollack and Chapman (1977). Lithosphere temperature structure is identified by surface heat flow.

3. Application of the model to continental intraplate lithosphere

The mathematical model described above gives the response of the lithosphere to a given applied stress in terms of its stress evolution with time and depth. Figure 3 shows stress/depth profiles at various times for lithosphere with a continental shield type geotherm with a heat flow of $q = 45$ m W m^{-2} (Fig. 3A) and a Basin-and-Range type geotherm with a heat flow of $q = 95$ m W m^{-2} (Fig. 3B). The lithosphere is subjected to an initial tensional applied stress of 0.2 kbar.

As time increases, ductile creep in the lower lithosphere leads to the decay of stress there and its transfer to the upper lithosphere. In the continental shield lithosphere, by 10^6 y, stress decay in the lower lithosphere is almost complete and the level of stress in the upper lithosphere has increased to $\sim \times 2$. Brittle fracture in the topmost lithosphere has also occurred resulting in downwards stress transfer. With increase in time, the high ductility zone at the base of the lower crust (where quartz rheology overlies olivine) becomes more pronounced. Higher levels of stress produce a similar stress distribution but in a shorter time.

In the hotter Basin-and-Range type lithosphere, stress decay in the mantle and lowermost crust is almost complete by 10^3 y and stress has been amplified in the middle crust by a factor of $\times 8$. Two subsidiary stress maxima occur at ~ 20 and 35 km depth corresponding to the discontinuities in rheology as the composition changes from wet to dry quartz and from dry quartz to olivine. At 10^4 y the brittle failure envelope has intersected the top of the region in which ductile deformation has occurred, resulting in a sharp stress peak (at 10 km). The elastic core of the lithosphere for this model has therefore ceased to exist by this time, with all of the lithosphere experiencing significant brittle or ductile deformation—i.e., *Whole Litho-*

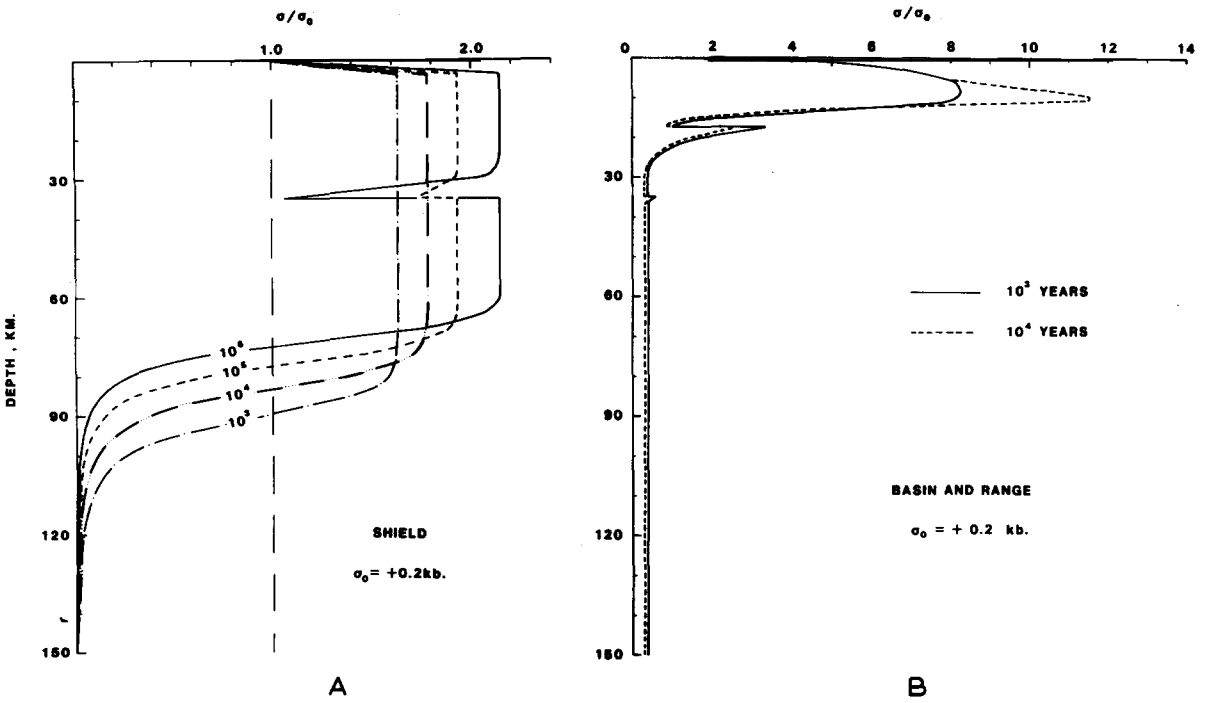

Fig. 3. Horizontal stresses within continental lithosphere versus depth at various times after the application of an initial stress $\sigma_0 = +0.2$ kbar. A—Shield type lithosphere; B—Basin and Range Type Lithosphere.

sphere Failure (WLF) is about to take place (cf. Fig. 1B).

A comparison of Fig. 3A with 3B demonstrates that the temperature structure of the lithosphere, because of its effect on lithosphere rheology, is critically important in controlling not only the time taken for WLF to occur, but also the rate at which subsequent deformation takes place (Kusznir and Park, 1982). Figure 4A shows strain versus time for models with different heat flow values ranging from $q = 40$ to $q = 100$ m W m^{-2}. The temperature structures were calculated using the continental lithosphere temperature model of Pollack and Chapman (1977). For a tensile applied stress of 0.2 kbar, WLF occurs at $\sim 10^3$ y in lithosphere with $q = 80 - 100$ m W m^{-2}. For cooler lithosphere with $q = 60$ m W m^{-2}, WLF occurs later, at $\sim 10^5$ y. For a compressional applied stress of 0.2 kbar a heat flow of at least 80 m W m^{-2} is required to produce WLF by 10^6 y.

Figure 4B shows the effect of increasing the initial applied stress for lithosphere with an intermediate temperature structure ($q = 60$ m W m^{-2}). WLF occurs at 10^5 y for a tensile applied stress of 0.2 kbar and for a compressive applied stress of 0.5 kbar, which demonstrates that, as would be expected, the lithosphere is much stronger under compression than under tension. It is clear from Fig. 4A and B that geologically significant strains of $> 1\%$ in c. 1 Ma (i.e., strain rates $> 10^{-15}$ s^{-1}) will occur only for hotter lithosphere or under rather large applied stresses.

It follows from the above that, for any given value of heat flow, there will be a critical threshold value of both tensional and compressional applied stress which will cause WLF in a given time and thereby initiate large, geologically significant strains. Figure 5 summarises the relationship between the critical stress σ_c required to cause WLF in 1 Ma and heat flow q, indicating the fields in which significant deformation is predicted. The diagrams can be used to calculate, for a region of continental lithosphere with known heat flow, the critical applied stress necessary to cause significant

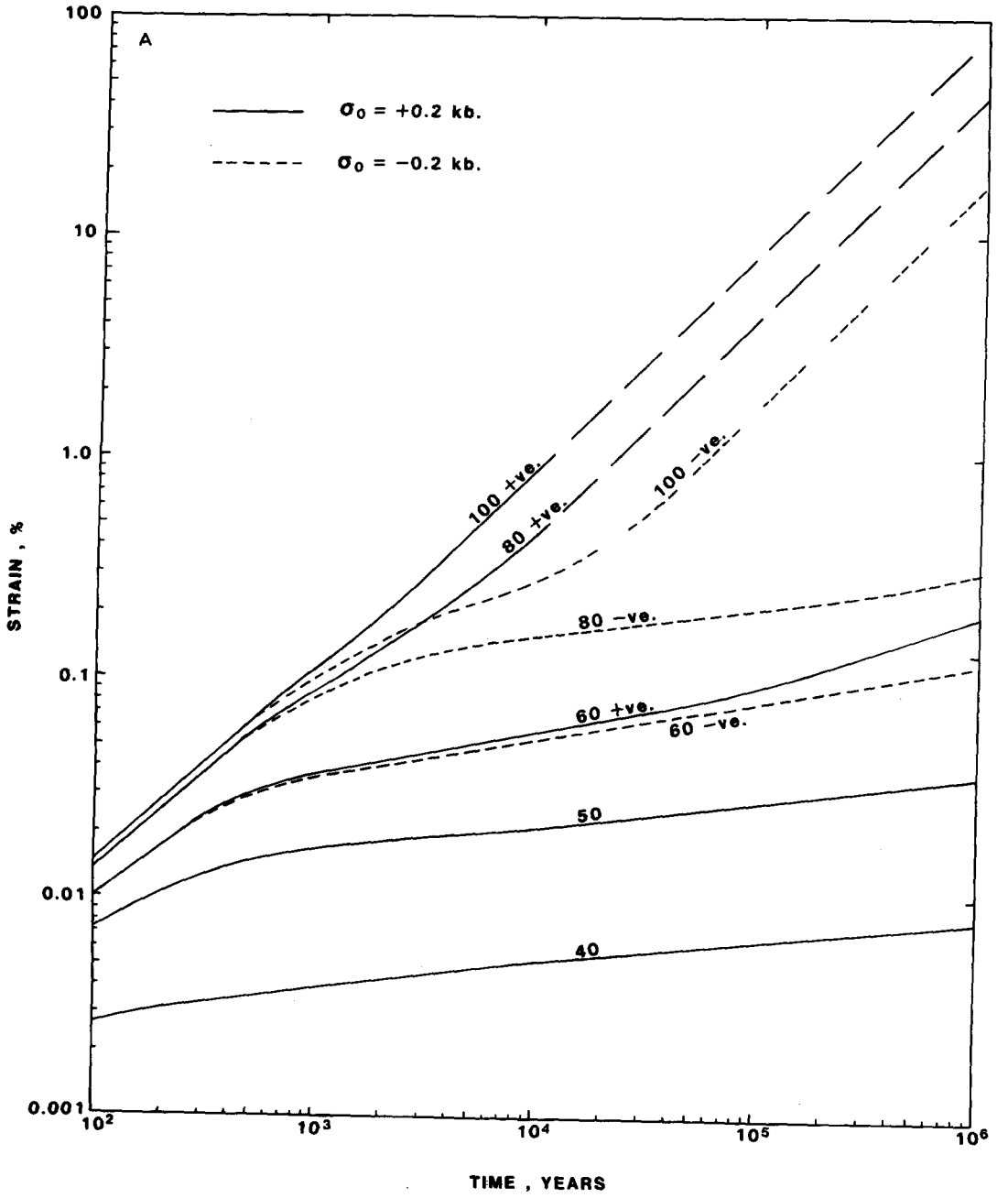

deformation. The critical stress σ_c is sensitive to small changes in q in the range 40–80 m W m^{-2}. Weakening the model failure strength by choosing a much lower value of T_0 has the effect of lowering σ_c significantly in this region, but changes in the value of the coefficient of friction μ have a much smaller effect relatively.

Figure 5A also indicates the theoretical stress levels associated with the main sources of tensional intraplate stress (plateau uplift, subduction

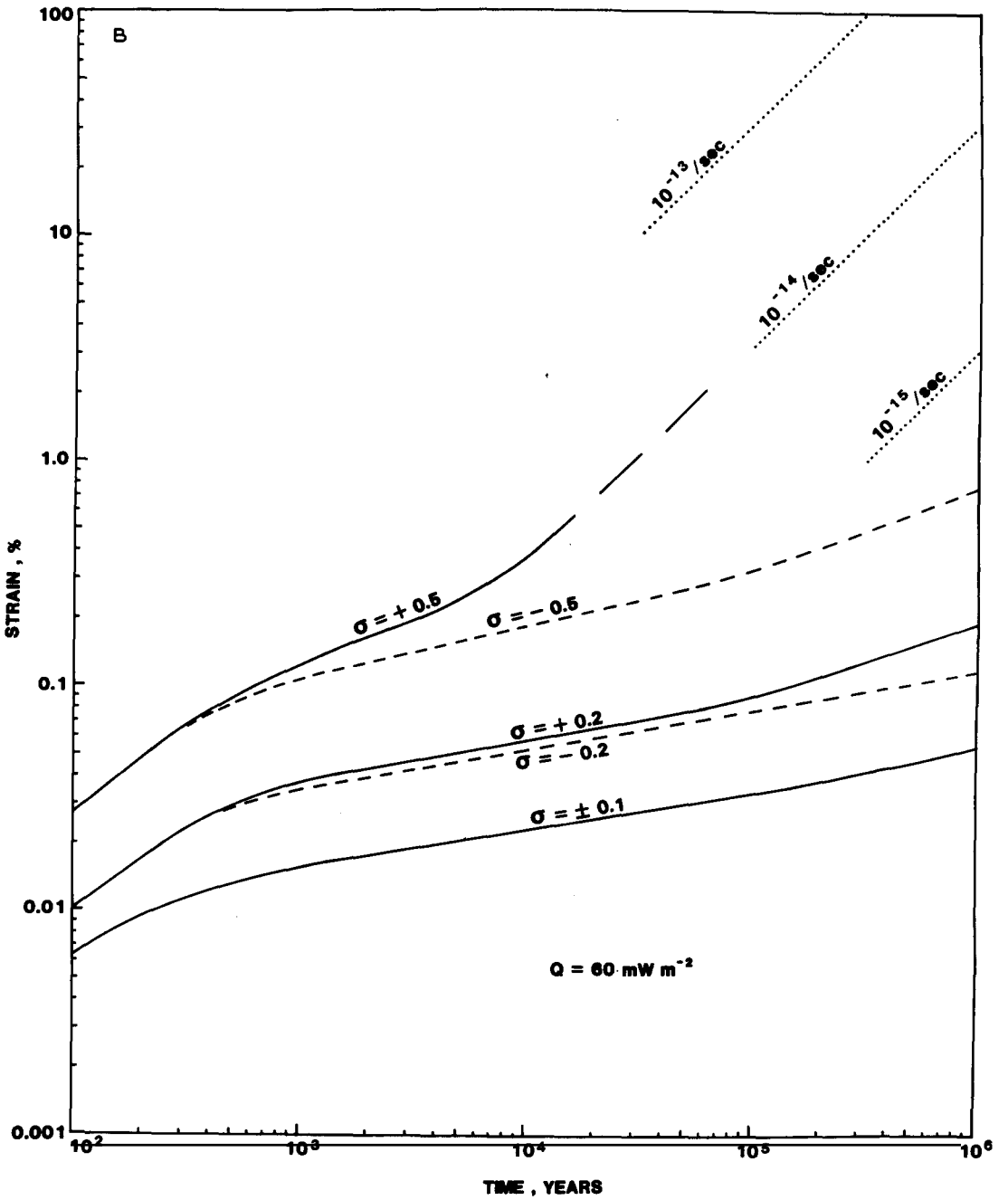

Fig. 4. Strain-time curves for continental lithosphere. (A) The response of lithosphere with different geothermal structures (characterized by their heat flow values measured in m W m^{-2}) for an applied stress σ_0 of ± 0.2 kbar. (B) The response of lithosphere with a heat flow of 60 m W m^{-2} subjected to applied stresses of ± 0.1, ± 0.2 and ± 0.5 kbar. Strain rates in the geologically significant range 10^{-13}–10^{-15} are shown for comparison.

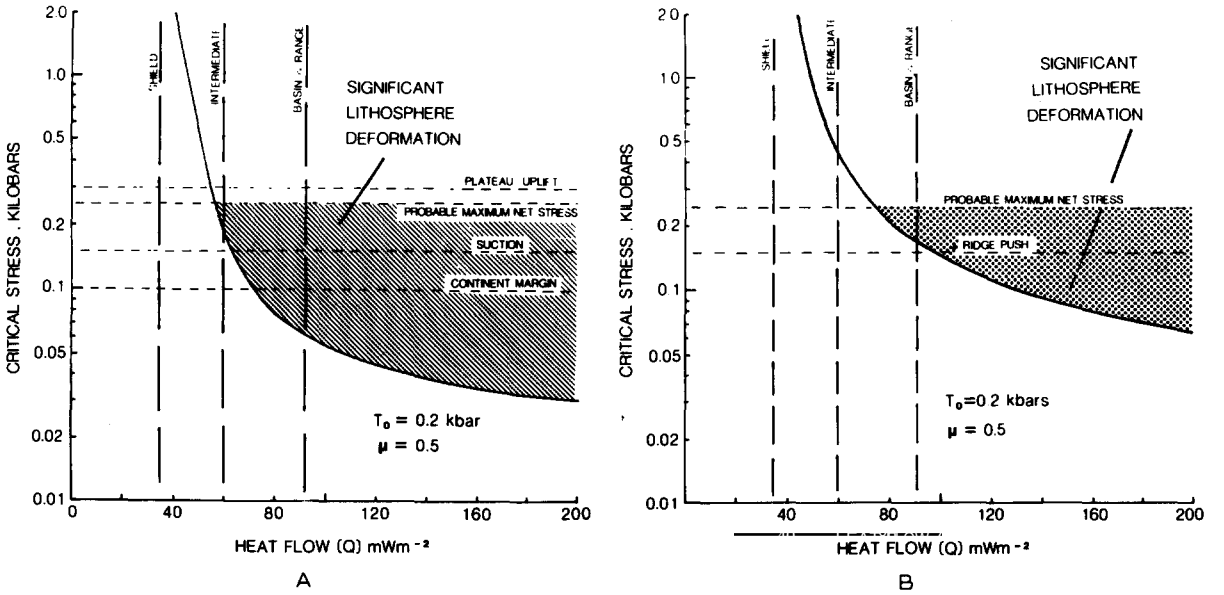

Fig. 5. Critical stress σ_c versus lithosphere heat flow for (A) tensional and (B) compressional applied stress. Likely levels of intraplate stress arising from plate boundary sources and compensated load structures are shown for comparison together with expected maximum net available stresses. Fields of significant lithosphere deformation are represented by ornamented regions.

suction and continent margin effects – see Table I). In practice, these tensional stresses would be partly offset by compressional stresses and it is unlikely that in present-day continental lithosphere a net (renewable) tensional stress exceeding 0.25 kbar exists, although locally this level could be exceeded due to contributions from non-renewable stresses (e.g., thermal or membrane stresses).

In the case of compressional deformation (Fig. 5B) the likely maximum net stress level may be of the same order but would only be achieved in a piece of continental lithosphere affected by an adjacent plateau uplift supplementing the ridge push force.

In the above calculation the critical stress required to generate WLF by 1 Ma has been determined. The critical stress required to generate failure will decrease with an increase in the time to WLF. However, the model does predict a finite strength for the lithosphere over the geological time scale.

Not considered in the model is the alteration of the geothermal gradient by lithosphere deformation. Compressional deformation, leading to lithosphere thickening, will give a reduction in the geothermal gradient and a strengthening of the lithosphere. In contrast extensional deformation will result in thinning of the lithosphere and an increase in the geothermal gradient which will further weaken the lithosphere.

4. Brittle–ductile transition depth and its dependence on lithosphere temperature structure

The application of an applied stress to the lithosphere results in ductile deformation in the lower lithosphere and brittle deformation in the upper lithosphere. Prior to WLF these deformation regions are separated by a region of purely elastic deformation but at the moment of WLF and afterwards the regions of brittle and ductile deformation meet. This is illustrated in Fig. 1A and B. The point in depth at which the region of brittle and ductile deformation converge is the brittle–ductile transition.

The depth of the brittle–ductile transition is dependent on the lithosphere temperature struc-

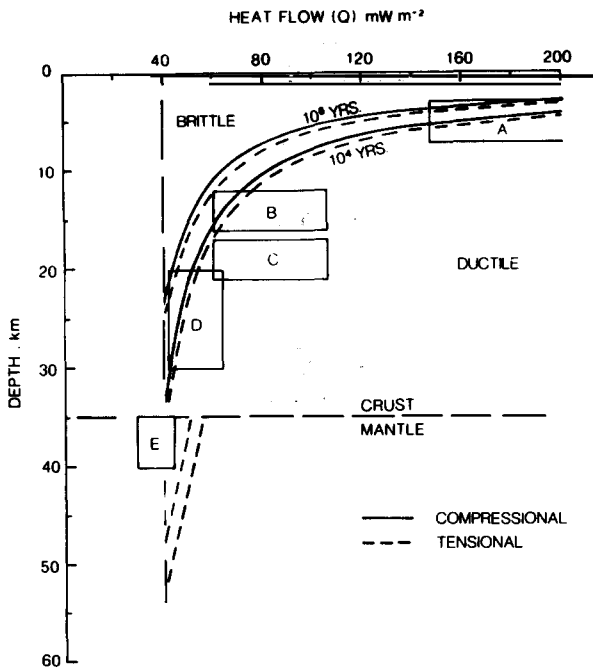

Fig. 6. The calculated depth of the brittle–ductile transition as a function of lithosphere heat flow for tensional and compressive deformation. Upper curves correspond to *Whole Lithosphere Failure* (WLF) by 1 Ma—lower curves to WLF by 10^4 y. Seismic estimates of the depth of the brittle–ductile transition as a function of heat flow are also shown for comparison. Seismic data areas are: (a) Geysirs and Clearlake Highlands; (b) Central California and Coso Range; (c) Wasatch Front; (d) Eastern U.S. and Canada; and (e) Sierra Nevada. Seismic evidence is adapted from Sibson (1982).

ture and can be determined from the lithosphere deformation model. Figure 6 shows the depth of the brittle–ductile transition as predicted by the model as a function of lithosphere heat flow. The depth of the brittle–ductile transition can be seen to decrease with increase in heat flow. Tensile deformation produces a slightly deeper brittle–ductile transition depth than compressional deformation. The upper curves of Fig. 6 correspond to WLF after 1 Ma, and the lower curves correspond to WLF by 10^4 y. The effect of increasing the strain rate (i.e., decreasing the time to WLF) is to lower the brittle–ductile transition depth.

Figure 6 also shows for comparison estimates of the brittle–ductile transition depths based on observations of the depth distribution of some continental intraplate earthquake foci as a function of heat flow. The data are taken from Sibson (1982). The brittle–ductile transtion depth is estimated by assuming that it corresponds to the greatest depth of observed seismic foci. Focal mechanisms correspond to extensional, thrust and strike slip faulting. A similar relationship is seen between the brittle–ductile transition depth and heat flow for the observed data as shown by the model. The seismic data, however, correspond better to the faster strain rate models.

5. Discussion

The lithosphere deformation model predicts significant extensional deformation in continental regions with heat flow values $q >$ c. 60 m W m^{-2} given a favourable combination of stress sources, and significant compressional deformation in regions with $q >$ c. 75 m W m^{-2} under rather restricted conditions of stress combination. For more usual levels of compressive stress (cf. the ridge-push estimate of 0.15 kbar) failure would only occur in hot or weak lithosphere. These predictions can be compared with the heat flow data and tectonic status of a number of representative regions (Table II) divided into (A) *continental shield* (Precambrian cratons) (B) "*intermediate*" (Palaeozoic orogenic crust) and (C) *thermally "active"* (areas of current or recent rifting and volcanicity). None of Group A with heat flow values in the range 34–49 m W m^{-2} show signs of significant current deformation (taking "significant" to mean showing lateral crustal strains of c. 1% or more). In Group B, with values of q in the range 57–75 m W m^{-2}, extensional failure is taking place in the Rhine–Ruhr rift system in central Europe west of the Bohemian massif, and in the Shansi graben system of northern China. In group C, high heat flows ($q >$ 90 m W m^{-2}) are associated with active volcanicity and extensional rifting. The data are therefore in broad agreement with the predictions of the model. However, it is important to stress that the model ought strictly to be applied only to the initial stage of rifting, starting from "normal" lithosphere. Once significant crustal thinning has taken place, both the geometry and the rheology of the lithosphere

TABLE II

Region	Heat flow, m W m^{-2}	Deformation state
A. Shield		
Superior Province [2]	34 ± 8	no failure
West Australia [2]	39 ± 8	no failure
West Africa (Niger) [2]	20 ± 8	no failure
South India [2]	49 ± 8	no failure
Mean Archean + older Proterozoic [5]	41 ± 10	no failure
B. Intermediate		
Eastern U.S.A. [2]	57 ± 17	no failure
England and Wales [2]	59 ± 23	no failure
Central Europe (Bohemian massif) [2]	73 ± 18	local failure
Northern China [1]	75 ± 15	local failure
Mean Younger Proterozoic [5]	50 ± 5	–
Mean Palaeozoic [5]	62 ± 20	–
C. Thermally active		
Rhine graben [3]	107 ± 35	extensional failure
(flanks—Rhenish massif) [3]	(73 ± 20)	
Baikal rift [3]	97 ± 22	extensional failure
(S.E. flank—Older Palaeozoic) [3]	(55 ± 10)	
East African rift [3]	105 ± 51	extensional failure
(flanks) [3]	(52 ± 17)	
Basin-and-Range Province [2]	92 ± 33	extensional failure
(E. flank—Colorado plateau) [4]	(60)	

Heat flow data from Pollack and Chapman (1977) [1], Vitorello and Pollack (1980) [2], Morgan (1982 [3], 1983 [4], in press [5]).

are changed by the emplacement of warmer lithosphere material in the lower part of the lithosphere (cf. McKenzie, 1978) and in many cases by the development of volcanicity. These changes result in an increased thermal gradient which will in turn cause further structural weakening. The heat flow in an active rift would then be expected to be rather higher than in surrounding areas (e.g., compare the values of 107 ± 35 m W m^{-2} for the south Rhine graben with 73 ± 20 m W m^{-2} for the Rhenish massif—Table II). The data of Table II can therefore be used to give broad confirmation that the threshold values of heat flow predicted by the model are correct—i.e., the values for areas which have not suffered failure may be taken as minimum threshold values while these which have suffered failure indicate maximum values. It may be concluded that the model predictions are in good agreement with stress estimates and heat flow data for areas of extensional intraplate deformation.

Examples of Mesozoic–Tertiary extensional rift systems (e.g., the Rhine and Baikal rifts and the Basin and Range province) show extensional strains in the range 10–100% over time periods of the order of 10–100 Ma, giving average strain rates of 10^{-16}–10^{-15} s^{-1} (Kusznir and Park, 1984). The strain-time curve for 0.2 kbar tension with a heat flow of 60 m W m^{-2} (Fig. 4) might be taken as a representative set of conditions leading to rifting. This curve shows WLF at $\sim 10^5$ y, but it is clear by extrapolation that probably several tens of Ma will elapse before a geologically measurable strain of ~ 1% is reached. The implication is that geological evidence of intraplate extension may not appear until many tens of Ma after the imposition of the stress in lithosphere with average heat flow. The critical stress values for Fig. 5 represent the stress required to produce WLF in 10^6 y. The stress levels responsible for many real rift systems would probably be higher, to produce visible results in a geologically appropriate time scale.

Significant compressional intraplate deformation seems to be uncommon at present. Examples occur in Central Asia north of the Himalayan collision zone between India and Asia (Molnar and Tapponnier, 1975). Figure 5B would suggest that, with a likely heat flow in the range 60–70 m W m^{-2}, rather large stresses of -0.3 to -0.45 kbar would be required to initiate the deformation. Such stresses are too large to be produced by ridge-push alone. Larger compressive stresses could have arisen from the contribution of the Himalayan–Tibetan plateau uplift. Alternatively (or additionally) the deformation may have been localised in zones of anomalously high heat flow or weak crust.

References

Bodine, J.H., Steckler, M.S. and Watts, A.B., 1981. Observations of flexure and the rheology of the oceanic lithosphere. J. Geophys. Res., 86: 3695–3707.

Bott, M.H.P., 1982. Origin of the lithosphere tension causing basin formation. Philos. Trans. R. Soc. London, Ser. A: 305: 319–324.

Bott, M.H.P. and Kusznir, N.J., 1979. Stress distributions associated with compensated plateau uplift structures with application to the continental splitting mechanism. Geophys. J.R. Astron. Soc., 56: 451–459.

Bott, M.H.P. and Kusznir, N.J., 1984. Origins of tectonic stress in the lithosphere. Tectonophysics, 105: 1–13.

Forsyth, D. and Uyeda, S., 1975. On the relative importance of the driving forces of plate motion. Geophys. J.R. Astron. Soc., 43: 163–200.

Goetze, C., 1978. The mechanism of creep in olivine. Philos. Trans. R. Soc. London, Ser. A: 288: 99–119.

Heard, H.C., 1976. Comparison of the flow properties of rocks at crustal conditions. Philos. Trans. R. Soc. London, Ser. A: 283: 173–186.

Koch, P.S., Christie, J.M. and George, R.P., 1980. Flow law of "Wet" Quartzite in the α-Quartz Field. Trans. Am. Geophys. Union, 61: 376.

Kusznir, N.J., 1982. Lithosphere response to externally and internally derived stresses: a viscoelastic stress guide with amplification. Geophys. J.R. Astron. Soc., 70: 399–414.

Kusznir, N.J. and Bott, M.H.P., 1977. Stress concentration in the upper lithosphere caused by underlying viscoelastic creep. Tectonophysics, 43: 247–256.

Kusznir, N.J. and Park, R.G., 1982. Intraplate lithosphere strength and heat flow. Nature, 299: 540–542.

Kusznir, N.J. and Park, R.G., 1984. Intraplate Lithosphere Deformation and the Strength of the Lithosphere. Geophys. J.R. Astron. Soc., 78.

McClintock, F.A. and Walsh, J.B., 1962. Friction on Griffith cracks under pressure. Fourth U.S. Natl. Congr. Appl. Mech. Proc., pp. 1015–1021.

McKenzie, D.P., 1978. Some remarks on the development of sedimentary basins. Earth Planet. Sci. Lett., 40: 25–32.

Mithen, D.P., 1982. Stress amplification in the upper crust and the development of normal faulting. Tectonophysics, 83: 259–273.

Molnar, P. and Tapponnier, P., 1975. Cenozoic tectonics of Asia: effects of a continental collision. Science, 189: 419–426.

Morgan, P., 1982. Heat flow in rift zones. In: G. Palamason (Editor), Continental and Oceanic Rifts. Am. Geophys. Union, Geodynamics Series, 8.

Morgan, P., 1983. Uplift of the Colorado plateau and its relationship to volcanism and rifting in the adjacent Basin-and-Range and Rio Grande rift. Proc. XVIII General Assembly Int. U. Geodesy Geophys., Hamburg, p. 576 (Abstract).

Morgan, P., 1984. The thermal structure and thermal evolution of the Continental Lithosphere. Phys. Chem. Earth, in press.

Pollack, H.N. and Chapman, D.S., 1977. On the regional variation of heat flow, geotherms and lithosphere thickness. Tectonophysics, 38: 279–296.

Post, R.L., 1977. High temperature creep of Mt. Burnet Dunite. Tectonophysics, 42: 75–110.

Richardson, R.M., Solomon, S.C. and Sleep, N.H., 1976. Intraplate stress as an indicator of plate tectonic driving forces. J. Geophys. Res., 81: 1847–1856.

Sibson, R.H., 1982. Fault zone models, heat flow, and the depth distribution of earthquakes in the continental crust of the United States. Bull. Seismol. Soc. Am., 72: 151–163.

Turcotte, D.L. and Oxburgh, E.R., 1976. Stress accumulation in the lithosphere. Tectonophysics, 35: 183–199.

Vitorello, I. and Pollack, H.N., 1980. On the variation of continental heat flow with age and the thermal evolution of continents. J. Geophys. Res., 85: 983–995.